Astron. Astrophys. 344, 965–972 (1999)

ASTRONOMY AND ASTROPHYSICS

Average properties and temporal variations of the geometry of solar network cells

F. Berrilli[1], **I. Ermolli**[2], **A. Florio**[2], **and E. Pietropaolo**[3]

[1] Università degli Studi "Tor Vergata", Viale della Ricerca Scientifica, I-00133 Roma, Italy
[2] Osservatorio Astronomico di Roma, Viale del Parco Mellini, 84, I-00136 Roma, Italy
[3] Università degli Studi, Via Vetoio, Località Coppito, I-67010 L'Aquila, Italy

Received 31 March 1998 / Accepted 26 June 1998

Abstract. The average properties of the network cells geometry and their temporal variations are investigated for quiet solar regions at the center of the solar disk. These regions were extracted from the daily Ca II K full-disk observations carried out at the Rome Observatory with the PSPT telescope during one year (from July 1996 to June 1997) at the beginning of Solar Cycle 23.

We applied an automated procedure to derive the skeleton of bright Ca II K regions. By using this skeleton as representative of the chromospheric network, we identified and characterized the network cells on the images.

The results we found seemed to point out that network cells are regular in shape and slightly flat. We found an upper limit of 2% for the anisotropy of the cell orientation. By analyzing the latitudinal dependence of the cell size, we found that the cell area decreases by about 30% towards the poles.

We also characterized the network pattern by using wavelet analysis. We compared the results obtained by the different analyzes.

Finally we analyzed the temporal behaviours of the network cell geometrical properties. In particular, we found a decrease of the characteristic scale value of about 8% for the period analyzed.

Key words: techniques: image processing – Sun: activity – Sun: chromosphere

1. Introduction

Recently, there has been a renewed interest in the chromospheric network.

This interest was raised at first by the results obtained on the solar irradiance variability. In fact it has been established that magnetic features are the primary sources of the solar irradiance variability (Lean 1997; Livingston et al. 1991). To develop consistent models of the solar activity cycle it is important to know in detail how the solar magnetic field varies and the mechanisms responsible for its variations, besides the fact that the properties of the magnetic features should be known.

Send offprint requests to: I. Ermolli (ilaria@oarhp1.rm.astro.it)

A detailed knowledge of the network properties is also necessary to get insights about the physical processes occurring in the solar interior.

For example, it is known that models developed to describe the interaction between solar rotation and the turbulent convective flows predict the existence of a latitudinal dependence of the convective energy flux (Gilman 1981; see the review by Spruit et al. 1990). The supergranules, i.e. the network pattern, that represents a convective phenomenon originating in the deeper layers of the convection zone, is the most promising candidate for showing such an effect. It should produce a latitudinal dependence of the cell size.

Another interesting topic is the understanding of the discrepancy among different estimated coefficients describing the dispersal of the magnetic field. The length scale and the topology of the network pattern affect the dynamical behaviour of the magnetic field and characterize its dispersal.

Besides the interest to get a precise knowledge of the network properties and despite the intensive study of the active regions (see the review by Semel et al. 1991), the properties of the magnetic network have been studied accurately only in the most recent years. This was mainly due to the uncertainty and the difficulty in identifying and characterizing the network.

A large part of the results obtained to date were obtained by applying statistical autocorrelation analyzes on dopplergrams and magnetograms and by measurements of visually identified cells on drawings of the network pattern obtained by enlargements of Ca II K spectroheliograms. The network cell properties inferred by these analyzes were largely dependent on the chosen method of analysis and are strongly affected by the visual identification of the cells.

Supergranulation, i.e. the chromospheric network cell pattern, is usually quoted to have a typical length scale of ≈ 30 Mm, as first stated by Simon & Leighton (1964). However, it has been found that this cell pattern exhibits a large dispersion in the individual cell sizes. It is also known that the area of the network elements is anticorrelated with solar activity: there is an enhancement in the cell dimension at the solar minimum (Singh & Bappu 1981; Kariyappa & Sivaraman 1994).

Contrasting results have been reported on the cell shape. By a cross correlation analysis of some Ca II K Arcetri spectrohe-

liograms, Sykora (1970) showed that the East-West diameters of the cells are about 5% larger than the North-South ones. On the other hand, by statistically analyzing Ca II K NSO spectroheliograms, Loucif (1988) did not find any polar/equatorial anisotropy. Different results have been also reported about the latitude dependence of the network cell size. Brune & Wöhl (1982), Münzer et al. (1989), Komm et al. (1995) found a decrease of the cell size towards the poles. Rimmele & Schröter (1989) also confirmed this trend but found a minimum cell size at mid-latitudes.

Only in the most recent years different authors devoted increased efforts to the application of spectral analysis techniques and to the development of appropriate algorithms for automatically identifying the network pattern and accurately measuring their geometrical properties (Komm 1995; Berrilli et al. 1998, hereafter Paper I; Schrijver et al. 1997; Hagenaar et al. 1997). Different approaches involving the use of self-similarity techniques have been also applied to describe the geometry of the network pattern and to get insight about the processes that produce it (Laurence 1991; Laurence & Schrijver 1993; Balke et al. 1993).

All these authors pointed out that some cell properties seem to depend on the method of analysis. Different approaches can produce different evaluations of the average cell size and different distributions of the cell areas. Besides the interest to the understanding of these differences and to get a precise evaluation of the cell average size, it is important to evaluate the variations of the cell properties on the solar disk and their temporal variations.

In this paper we continue the analysis of the geometrical properties of the chromospheric network cells undertaken in Paper I. We improved the automated cell identification algorithms to analyze in detail some properties of the cell geometry, in order to point out relations between the physical processes occuring in the solar interior and the observational evidences.

Our analysis considers some statistical averaged properties of the cells (orientation, elongation, size, fractal dimension, characteristic scale), and the temporal dependence of some of these properties. We also analyze the dependence of cell dimension with the position on the solar surface. We compare some results obtained by the analysis of identified cells with those obtained by a spectral wavelet analysis of the images. We applied our analyzes to one year of daily Ca II K images obtained in a period of minimum solar activity at the beginning of Solar Cycle 23.

2. Observations and image processing

The images we analyzed are taken in the data archive of the daily observations carried out at the Rome Observatory with the PSPT telescope (Coulter & Kuhn 1994; Ermolli et al. 1998). 183 full-disk images of the Sun analyzed were acquired from July 1996 to June 1997 using a Ca K II interference filter (centered at 393.3 nm bandwidth = 0.25 nm) and a 1 K $\times$ 1 K CCD camera with a pixel size of ≈ 2 arc sec. A photometric accuracy of 0.1% per pixel was obtained by coadding 100 frames acquired with very short exposure times (usually, less than 50 ms).

The eleven months sequence of observations was interrupted only by bad weather conditions and telescope maintenance.

To study the average properties of the network cell geometry and their temporal variations we selected a 256 $\times$ 256 pixels sub-array centered on the solar disk. To describe the latitudinal dependence of the cell size we analyzed 3 full-disk images.

None of the images analyzed presents active regions and therefore we did not apply masks to remove spots or plages.

To each calibrated image available (i.e. dark-subtracted and flat-fielded) we applied a three-step numerical process to extract the geometrical properties of network cells.

First, we applied a 3 $\times$ 3 de-noising filter and FFT highpass filter to each image, in order to remove intensity limb-darkening and low frequency gradients incidentally produced by a poor flat-fielding correction.

Then we extracted the skeleton of bright Ca II K regions and used it as definition of the chromospheric network. This was accomplished by using an improved version of the algorithm described in Paper I. This new procedure uses the skeleton obtained by a two-level image (where pixels set to 1 are representative of the chromospheric network) as a starting pattern and iteratively modifies it producing a new skeleton by taking into account the intensity information contained in the Ca II K images. The threshold value we used to create the two level images was chosen to get an approximately constant (rms less than 10%) number of identified cells for every analyzed images.

The iterative process stops when the changes to a new skeleton became negligible to respect to the previous one. At the end of the skeletonizing process the 'peduncles' or branches present in the boundaries of the network cells, that produce overstimated perimeter values, are pruned using a cellular automaton filter (ACF). In Fig. 1 we show an original image (left) and the same image with the corresponding skeleton superimposed (right).

The final step of our procedure is the identification of the cells and the measurement of the cell geometrical properties. Both tasks were accomplished by improved programs that identify the cells and calculate for each cell: area, perimeter, barycenter, dimension in the equatorial (E-W), polar (N-S) and diagonal directions (NE-SW and SE-NW), orientation and average radius to respect to the barycenter. We corrected the cell area and perimeter for geometrical projection effects.

We analyzed in this way a sample of about 60000 cells with a scale greater than 5 Mm. The cell scale is defined as the square root of the area of the cell.

The inferred geometrical properties of network cells depend on the identification method. In particular, as extensively discussed in Paper I, the skeletonizing algorithm can modify the shape of the detected cells or cause the merging of supergranules. The use of intensity information in our improved procedure largely reduces the cell boundary distortions introduced by the use of a single two-level image, and link adjacent domains that the previous numerical process did not identify. Nevertheless some connections could remain unresolved, pruned by the ACF, and then some supergranules still merge together. However, the

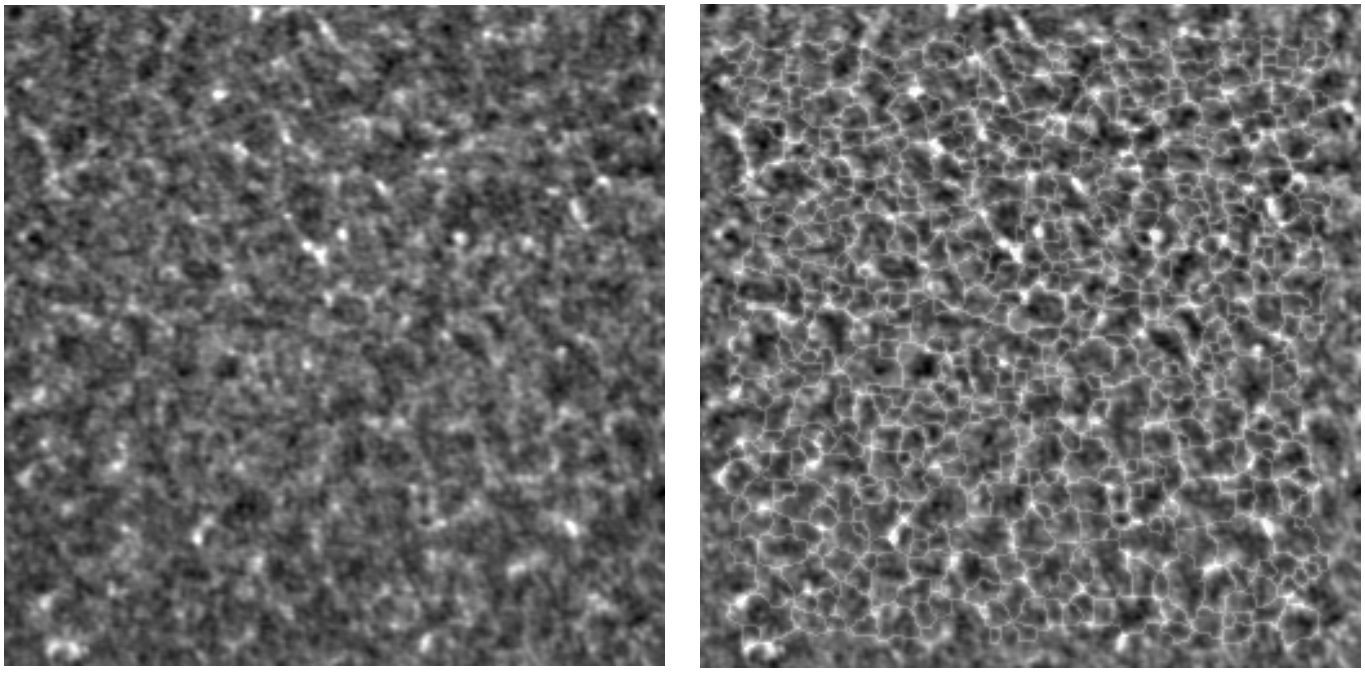

Fig. 1. *Left:* PSPT original calibrated sub-image (13 July, 1996). *Right:* Skeleton (light line) superimposed to the same sub-image.

redistribution of cell areas deriving from this process, as already discussed in Paper I, does not modify the essence of our conclusions. At the same time the randomness of the merging process and the high number of extracted cells make us confident about the morphological analysis presented in the next sections. With respect to the results presented in Paper I, we expect that the application of our new procedure permits a more precise description of the network cell perimeters, while producing only minor changes in the evaluation of the cell areas.

Table 1. Arithmetic mean of cell dimensions and percentage of cells (last row) oriented along polar, equatorial and diagonal directions.

direction	NS	NE-SW	EW	SE-NW
sample	18.8 Mm	18.5 Mm	18.8 Mm	18.7 Mm
rotated sample	18.8	18.2	18.5	18.7
good-seeing s.	17.4	17.2	17.6	17.4
percentage	28%	22%	26%	24%

3. Average properties of the cell geometry

3.1. Cell orientation

To search for a possible anisotropy in the cell orientation we calculated the arithmetic mean of the cell dimension in the four directions: polar, equatorial and diagonals for ≈ 8000 cells extracted from the images obtained on July 1996. We did not apply orbital or projection corrections on the extracted cells dimensions. In fact, the first ones (due to the excentricity of Earth orbit) are negligible for the analyzed sample due to solar ephemerides. The projection effects produce an axisymmetric deformation that flattens the cells by less than 2% for the cells on average. For a typical cell this is below the pixel size. Furthermore this does not introduce preferred directions. We expect that the combination of both effects produces only negligible changes in the shape of the cells.

The arithmetic mean values we obtained are reported in the first row of Table 1. These values indicate an upper limit for the anisotropy in the cells orientation of about 2%.

To check for possible effects introduced by the identification algorithm we also performed the same analysis on PSPT images rotated by 90 degree. The values we obtained, that are reported in the second row of Table 1, are in agreement within 2% with those reported for the right sample.

To evaluate possible seeing effects on the obtained results we also performed the analysis on a sub-sample of images obtained during good seeing conditions on July 1996. These images were selected by visual inspection and by searching the higher rms intensity values for very quiet solar regions (no presence of active remnants and bright points).

The results obtained by analyzing the "good seeing images" (≈ 2000 cells), reported in the third row of Table 1, confirmed a 2% upper limit for the anisotropy in the cell orientation and showed a contraction of about 4% in the mean values of the cell dimensions. This contraction is produced by an increase of the number of small cells extracted in good quality sub-images, also evident in the area distribution of cells discussed in the next subsection.

3.2. Cell size distribution

The distribution of network cell sizes is shown in the log N (number of cells) versus log S (cell scale) histogram (Fig. 2).

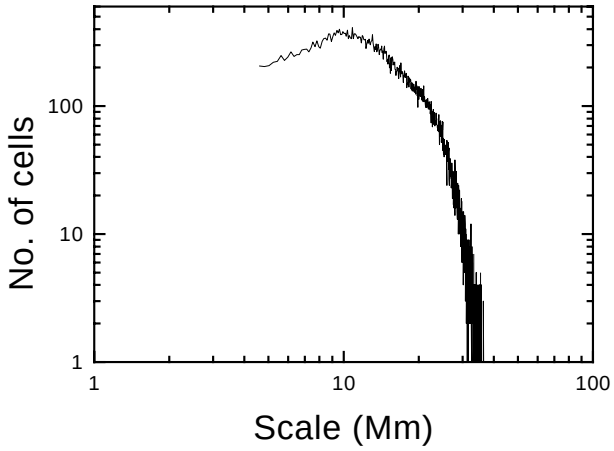

Fig. 2. Distribution of cell scale. We assumed as definition of the cell scale the square root of the area equivalent to the number of pixels included in the network cell.

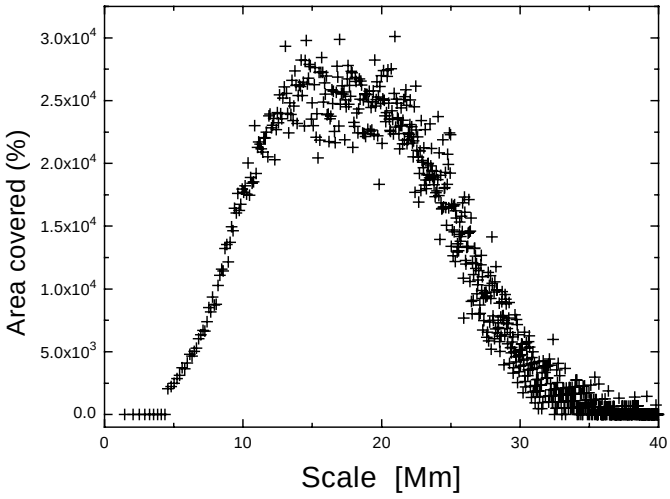

Fig. 3. Fractional contribution to the disk coverage by cells of different scale.

This histogram, composed of 700 bins, showed a continuous increase of the number of cells towards the smaller scales (10 Mm) and a change in the slope at a scale of about 24 Mm. As already reported in Paper I, the existence of this critical scale in the log-log plot suggests a transition between two regimes. With respect to the area distribution already showed in Paper I, we noted that the use of the new identification algorithms produced a change in the area distribution at the smaller scales ($\leq$ 10 Mm). This difference seemed to arise from a poor identification of cells without the use of intensity information. We stress that this difference exists only for the less significant cell scales.

The histogram obtained by the analysis of the selected sub-images shows an increase of the number of small network cells identified in good seeing condition images.

By using the size distribution we evaluate the percentage contribution to the disk coverage by cells of different scale, as showed in Fig. 3.

3.3. Cell shape

The orientation analysis we performed seemed to show a lack of anisotropic orientation of the network cells, at least for the cells located in the $500'' \times 500''$ region centered on the solar disk we analyzed. In order examine in detail the cell shape we now use two different geometrical cell describers.

The first we used is the fractal dimension D_f of the network cells, that can be derived from a log-log representation of the perimeter P - area A relation. D_f is given by:

$$\Delta P \approx \Delta A^{\frac{D_f}{2}}$$

where ΔP and ΔA represent the perimeter and area intervals where is found a linear correlation. In Paper I we estimated D_f = 1.35 for network cells with scales larger than the critical one. By the use of our improved skeletonizing algorithms we obtain D_f = 1.16 for cells with a scale greater than 24 Mm. This suggests that the new algorithms produce network cells which are more regular in shape.

We also calculate R for a Voronoi tesselation produced by using the barycenters of the $\approx$500 cells identified in a good quality image. We find D_f = 1.18 very close to the previous one. A Voronoi tesselation has been recently proposed by Schrijver et al. (1997) to describe the network cell pattern.

The result we obtained is different from that reported by Nesme-Ribes et al. (1996) who analyzed the facular magnetic pattern (D_f = 1.64). This difference, already reported in Paper I, can be due to the two different patterns analyzed or to the different identification criteria. In fact, while Nesme-Ribes, Meunier & Collin (1996) used an intensity threshold criterion to select the facular boundaries, we applied a skeleton algorithm (described in Paper I) that uses informations of the 8 neighbour pixels to identify the network cell perimeter. This permits the identification of boundaries that are more regular in shape.

In order to analyze the shape of the identified cells and to search for a possible average eccentricity and for a dependence of the shape with the cell size, we also use as the cell geometrical describer the ratio R between the longest dimension found in a cell and its orthogonal dimension. By analyzing the sample of more representative cells with scales from 12 to 26 Mm, we find R=1.46 $\pm$ 0.02. This value would be equal to 1 for circular cells.

The R value computed from the Voronoi tesselation (R = 1.47 $\pm$ 0.31) is very close to that obtained by analyzing the PSPT images.

The values we found seemed to point out that the network cells are quite regular in shape and slightly flat. Moreover, it seemed to be present a small dependence with the cell sizes, R increasing with the cell area.

3.4. Cell size dependence on heliographic latitude

As reported in Sect. 1 the results obtained to date showed a general decrease of the cell size towards the higher latitudes. As these earlier results were obtained by the use of spectral analyzes, we found interesting to use our automated cell iden-

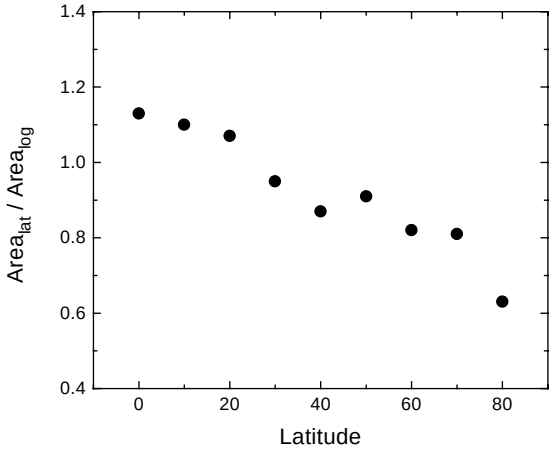

Fig. 4. Latitudinal dependence of the averaged cell area. The circles represent the ratio between the median value of the cell areas computed within 10^o latitude bins and the corresponding median value of the cell areas computed for the equatorial belt.

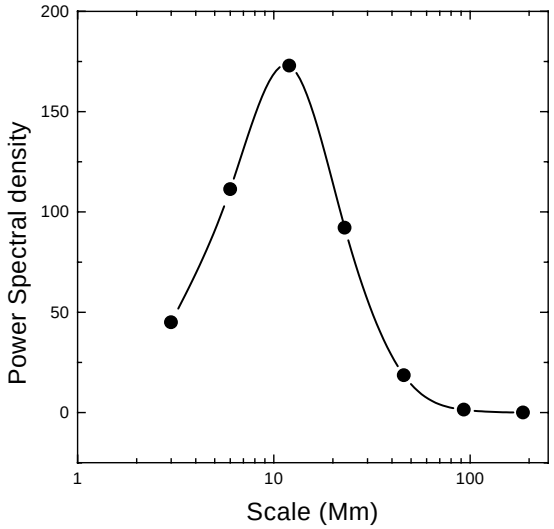

Fig. 5. The global spectrum computed for the PSPT sub-image obtained on 13 July, 1996. The circles represent energies as derived by the multiresolution analysis (arbitrary units). The line represents the spline interpolation used to find the scale at which the maximum of energy occurs.

tification procedure to evaluate the variation of cell size with heliographic latitude.

We have run our cell identification algorithm on 3 full-disk images for which the two ephemeris angles p and B_0 were minima (1.6% of the whole sample). The positions of the barycenters of the cells were determinated by the identification algorithms in cartesian coordinates, then transformed into heliographic coordinates. We did not distinguish between the northern and southern hemispheres and between the eastern and western hemispheres.

To compensate for geometrical foreshortening effects we assumed a constant size of the cells within the solar equatorial belt. In particular, we divided the scaling factors for the cells of the latitude intervals by those from the matching longitude intervals. In fact, the assumption of an inhomogeneous distribution of the cell size in longitude would imply a longitude dependent energy transport which is not very realistic.

We find that the median value of the cell areas decreases gradually by about 30% towards the poles, as showed in Fig. 4. We computed the median value of the cell areas because the distribution of the cell scale, that does not show the existence of a mean value of the cell scale (Fig. 2).

We obtained our result by analyzing the sample of cells with scale 10–30 Mm.

3.5. Wavelet analysis

Since the analysis on the identified cells showed a large spread in the individual cell sizes, we now try to characterize the network pattern by using the wavelet transform (for a review see Kumar & Foufoula-Georgiou 1997). An application of this analysis has been recently proposed by Komm (1995) to characterize the magnetic field pattern on solar magnetograms.

We improved his approach by using a bidimensional multiresolution analysis to characterize the network pattern on the PSPT images. This is a discrete wavelet transform that uses a distribution of scales organized in octaves, i.e. if the jth scale is 2^j, the next one is 2^{j+1}. This analysis also uses two sets of orthogonal wavelets functions; the first one, called the scaling function, is used to analyze and to represent approximations (in analogy to a low pass filter), the other one to represent details. This is sufficient to fully describe the analyzed function and eventually to reconstruct it. A proper combination of monodimensional scaling and wavelet functions permits the analysis of images, by the computation of three sets of coefficients for each scale, representative of the horizontal, vertical and diagonal directions respectively (Daubechies 1992).

We used the Haar function as the basic wavelet and the corresponding scaling function. We preferred the use of this simple largely applied function to favor simplicity and to get into account all the valuable scales, while loosing some refinements. In fact, the use of more smoothed functions produces ringing effects near the image borders for scales of the order of the image itself, thus limiting the number of valuable scales.

For each sub-image we computed the energy at the different scales by summing the squared coefficients for the horizontal and vertical directions at the different scales. These spans from the smallest one corresponding to ≈ 3 Mm up to the large one, corresponding to ≈ 371 Mm. As the diagonal direction gives a lesser contribution, we did not use it for this work. All the computed global spectra are distributed in a localized range of scales (from 46 Mm to 3 Mm) and show a maximum of power around the scale of 12 Mm (Fig. 5). To make evident the meaning of the wavelet scale we reported in Fig. 6 a typical PSPT sub-image and the eight relative images reconstructed by using the corresponding coefficients at a given scale. The reconstruction computed for the third level image, corresponding to a scale of 12 Mm, shows the most characteristic chromospheric feature.

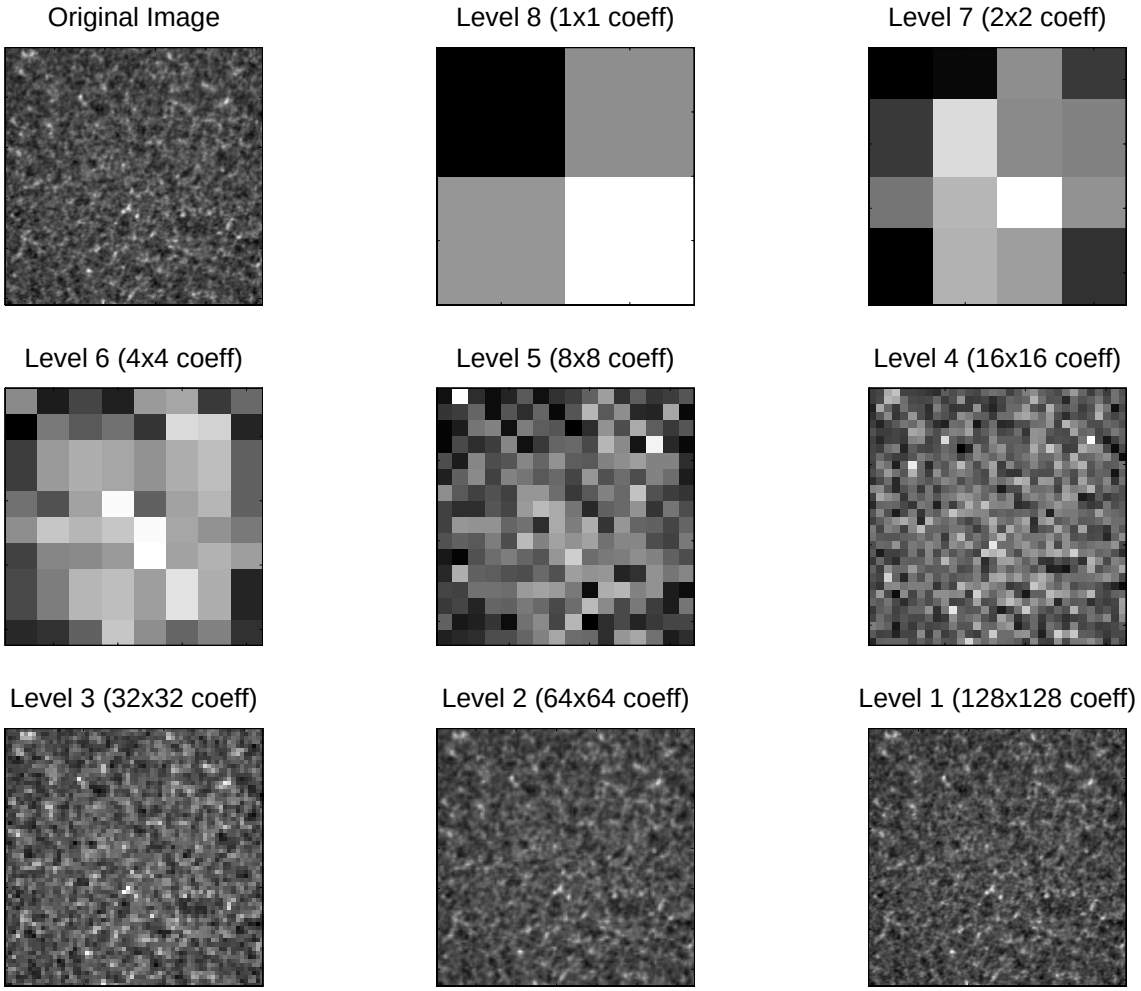

Fig. 6. Wavelet reconstruction for the PSPT sub-image obtained on 13 July, 1996. From top to bottom and left to right: the original image and the corresponding images reconstructed by using only the horizontal, vertical and diagonal coefficients at the labeled scales. The level 3 is the best realization between the reconstructed image quality and the number of wavelet coefficients used (32 for each direction).

4. Temporal variations of the geometrical properties of network cells

We now analyze the time dependence of the network cell geometrical properties.

For the analyzed period we report a slight decrease (Fig. 7) of the characteristic scale length, as derived from the wavelet analysis. The value of the characteristic scale was computed by applying a spline interpolation to each wavelet spectrum. The temporal dependence, that is corrected for effects of the excentricity of Earth orbit, was computed taking into account only monthly samples with at least five images.

The decrease of the network characteristic scale is also confirmed by a shift of about 0.9 Mm in the position of cell area distribution maxima computed for the monthly samples for July 1996 and May 1997.

The slight temporal dependence showed by our result is in agreement with the finding that the network cell size is anticorrelated with solar activity.

For the same period we also report a stability of the cell fractal dimension (Fig. 7). This result seems to suggest that the boundaries roughness of the cells is constant while their size decreases.

We stress that the period analyzed is around the minimum of the solar activity, at the beginning of Solar Cycle 23. Therefore the results we show about the temporal dependence of the different geometrical describers must be considered only as indicative of a possible time dependence. It would be very interesting to perform the same analysis with a larger sample of images obtained during a complete solar cycle.

5. Discussion

The analysis we performed on about 60000 identified cells pointed out that the network cells are quite regular in shape and lightly flat. We did not found evidence for anisotropy on the cell orientation larger than 2%. Our results showed that the network cells have a major axis, randomly oriented, on the average 1.4 times larger than the minor axis. By producing a Voronoi tesselation with the barycenters of cells on a good quality image, we found values for the describers of the cell geometry that are

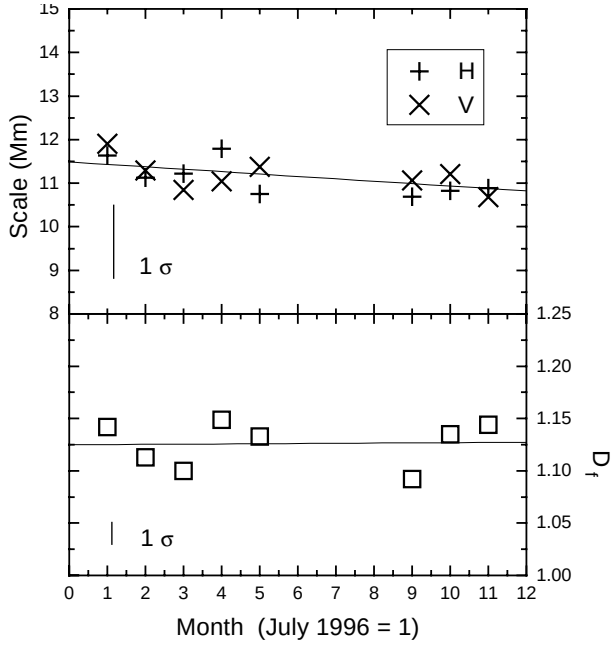

Fig. 7. Temporal variations of mean value of the wavelet characteristic scale calculated separately for the horizontal and vertical directions (*top*) and of the fractal dimension (*bottom*). The error bars represent the rms of the monthly averaged values. The lines represent the linear interpolation of the values.

close to those obtained by the analysis of the PSPT images. This suggests that the network cell shape is along irregular polygons, as recently also proposed by Schrijver et al. (1997) to describe the granular and supergranular cell pattern.

We confirmed the result of Paper I that the cell size distribution increases towards the smaller scales up to ≈ 10 Mm, further slightly decreases until a numerical cut-off (5 Mm). We found that the largest area contribution is given by cells with an average size of ≈ 20 Mm.

By analyzing the dependence of the median value of the cell areas from the heliographic position we found that the cell area (for cells with scale 10–30 Mm) gradually decreases by $\approx 30\%$ towards the poles. Our result, that is in agreement with some results already reported, is in qualitative accordance with the latitudinal dependence of the heat flux in the rotational models proposed by Gilman (1978). The magnitude of the variations in the heat flux required for the models is of the order of 20%. Our result is also in a quantitative agreement with this theoretical prediction, assuming that there is a linear dependence between the cell size and the mixing length (Weiss 1964).

We also tried to characterize the network pattern by using the wavelet analysis. The power spectrum computed for each analyzed sub-array shows the existence of a characteristic scale (≈ 12 Mm) where the maximum of power occurs. This result is in agreeement with the averaged size of the cell area distribution. This value is also in agreement with that reported by Komm (1995) by analyzing magnetograms.

For the analyzed period the geometry of the network cells seemed to show a slight systematic variation. In particular, the time behaviour computed for both the network cell size of the identified cells and the characteristic scale obtained by the wavelet analysis showed a slight decrease of the cell scale value. This result is in agreement with the finding that the network cell size is anticorrelated with the solar activity.

6. Conclusion

We have used a numerical procedure to extract the skeleton of regions selected to be representative of the chromospheric network, in order to analyze the averaged geometrical properties of the network cells and their temporal variations in a quiescent period of solar activity at the beginning of Solar Cycle 23 (from July 1996 to June 1997). The results we present about the cell shape and orientation are the first ones obtained by statistically analyzing identified cells, while the geometrical properties of the network cells were evaluated previously from autocorrelation and spectral analyzes. We stress that a detailed analysis of the network cell geometry can provide further observational constraints to the models of star rotation with turbulent compressible convection, besides the constraints provided by the helioseismology.

The time dependence we showed was obtained for a period around the minimum of the solar activity. Therefore our results are only indicative of a possible dependence. We plan to apply our analysis to a long period of solar PSPT observations, looking for the dependence of network cell geometry with the solar activity cycle. Meanwhile, we have undertaken the analysis of a sample of images obtained by the digitization of Ca II K spectroheliograms from different archives.

Acknowledgements. We thank M. Fofi (Rome Observatory) for the PSPT observations and the NSO/PSPT team (J. Khun, R. Coulter and H. Lin). We thank the referee Th. Roudier, whose comments have brought improvements on the text. Researches on the solar variability at the O.A.R. were partially supported by the Italian Government (Ministero dell'Ambiente).

References

Balke A.C., Schrijver C.J., Zwaan C., Tarbell T.D., 1993, Solar Physics 143, 215
Berrilli F., Florio A., Ermolli I., 1998, Solar Physics 180, 29
Brune R., Wöhl H., 1982, Solar Physics 75, 75
Coulter R.L., Kuhn J.F., 1994, In: Balasubramaniam K.S., Simon G.W. (eds.) Active Region Evolution: Comparing Models with Observations. ASP Conference Series, Vol. 68, p. 37
Daubechies I., 1992, In: Ten lectures on wavelets. CBMS - NSF, Regional Conference Series in Applied Mathematics, SIAM
Ermolli I., Fofi M., Bernacchia C., et al., 1998, Solar Physics 177, 1
Gilman P.A., 1978, Geophys. Astrophys. Fluid Dyn. 11, 157
Gilman P.A., 1981, In: NASA sp-450, The Sun as a star. p. 231
Hagenaar H.J., Schrijver C.J., Title A.M., 1997, ApJ 481, 988
Kariyappa R., Sivaraman K.R., 1994, Solar Physics 152, 139
Komm R.W., 1995, Solar Physics 157, 45
Komm R.W., Howard R.F., Harvey J.W., 1995, Solar Physics 158, 213
Kumar P., Foufoula-Georgiou E., 1997, Rev. of Geophys. 35, 385
Laurence J.K., 1991, Solar Physics 135,249
Laurence J.K., Schrijver C.J., 1993, A&A 411, 402

Lean J., 1997, ARA&A 35, 33
Livingston W., Donnelly R.F., Grigoryev V., et al., 1991, In: Cox A.N., Livingston W.C., Matthews M.S (eds.) The solar interior and atmosphere. The University of Arizona Press, Tucson, p. 1109
Loucif M.L., 1988, Compte Rendu Academie des Sciences 307, 1203
Münzer H., Hanslmeier A., Schröter E.H., Wöhl H., 1989, A&A 213, 431
Nesme-Ribes E., Meunier N., Collin B., 1996, A&A 308, 213
Rimmele T., Schröter E.H., 1989, A&A 221, 137
Schrijver C.J., Hagenaar H.J., Title A.M., 1997, A&A 475, 328
Semel M., Mouradian Z., Soru-Escaut I., et al., 1991, In: Cox A.N., Livingston W.C., Matthews M.S (eds.) The solar interior and atmosphere. The University of Arizona Press, Tucson, p. 844
Simon G.W., Leighton R.B., 1964, ApJ 140, 1120
Singh J., Bappu M.K.V., 1981, Solar Physics 71, 161
Spruit H.C., Nordlund A., Title A.M., 1990, ARA&A 28, 263
Sykora J., 1970, Solar Physics 13, 292
Weiss N.O., 1964, Phil. Trans. Roy. Soc. 256, 99